

EFFECT OF HIGH TEMPERATURE HEATING ON CHEMICAL COMPOUNDS IN MAGNESIUM COMPOSITE MATERIALS

Rezza Ruzuqi^{1*}, Eko Tavip Maryanto²

Fisheries Mechanization, Politeknik Kelautan dan Perikanan Sorong, Sorong City, Indonesia¹

Civil Engineering, Universitas Muhammadiyah Sorong, Sorong City, Indonesia²

rezza.ruzuqi31@gmail.com

Received : 29 November 2023, Revised: 20 March 2024, Accepted : 23 March 2024

*Corresponding Author

ABSTRACT

The development of magnesium composite-based seawater battery anode technology is actively pursued, especially in its ability to transmit and store electrical energy. However, many overlook the possibility that significant temperature changes during the process may lead to chemical compound alterations, potentially affecting the battery's performance. Therefore, this research examines the changes in chemical compounds in magnesium composite-based seawater battery anodes caused by high temperatures. In this study, the synthesis process of magnesium composite material composed of MgAlSnMn with variations of Manganese (wt.-%) 14.8, 15, 15.2, 15.4, 15.6. Then it was milled for 60 minutes. Next, the materials were pelletized using a manual compacting machine with a diameter and compressive strength of 10 mm and 150 kg/cm² respectively. After that, all materials were sintered at 750°C with a muffle furnace for 60 minutes. In this study, XRD equipment was utilized to determine chemical compound changes. The results indicate that magnesium composite materials undergo significant chemical compound alterations at high temperatures, including MgO (Magnesium Oxide Periclase), Al₁₈Mg₃Mn₂, and the remaining Al elements. This could potentially disrupt the performance of seawater batteries when applied. It is hoped that further research will be conducted in the future to enhance the quality and performance of the product.

Keywords : Seawater Battery , Magnesium Composites, Chemical Compound, High Temperatures

1. Introduction

Composite magnesium material is a type of material consisting of magnesium and other reinforcing materials combined to create a combination of desired properties. The magnesium composite matrix is a promising structural material, considering its high strength and modulus, but its poor ductility limits its application to a high degree. To achieve the required material quality, several treatments need to be performed, such as controlling material defects. Thus, the resulting magnesium alloy product has the highest strength ever achieved (Wu et al., 2017). Figure 1. illustrates the good magnesium product outcomes through several processes. Composite magnesium material also exhibits good cyclic strength when subjected to controlled uniaxial asymmetric stress (Yan et al., 2018).

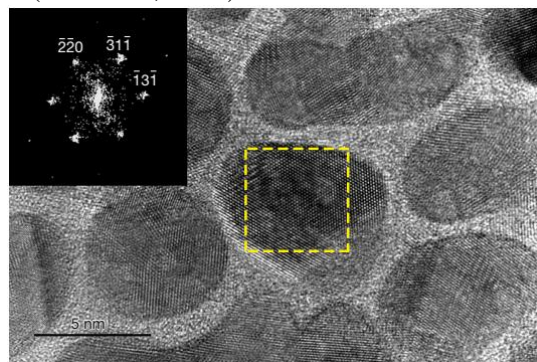


Fig. 1. Good Yield of Magnesium Products

Furthermore, the use of magnesium composite material becomes relevant because it can produce lightweight products while remaining strong and resistant to various environmental conditions. In addition to having these material characteristics, another characteristic of magnesium alloy is its good corrosion resistance to organic matter and alkalinity (Xu et al.,

2019). Therefore, the utilization of such material is also applied in the medical field (W. Yu et al., 2019).

Furthermore, aside from being applied in the medical field, the use of magnesium alloy material is also employed in various industries such as aerospace, railways, automotive, and maritime structures by combining additional materials such as aluminum (Singh et al., 2020). Since composite material is vital in various industries, specialized equipment and methods are required to cut the material to produce good surface properties, namely with cryogenic machining methods (Pu et al., 2012).

X-ray diffraction is a non-destructive material testing technique that provides detailed information about crystallographic structure, including crystal systems (cubic, tetragonal, orthorhombic, rhombohedral, hexagonal, monoclinic, triclinic), crystal quality (single crystal, polycrystalline, and amorphous), crystal symmetry, determination of crystal defects, determination of crystal parameters (lattice parameters, atomic spacing, number of atoms per unit cell), mixture identification, and chemical analysis (Holder & Schaak, 2019). Figure 2. shows a graphical representation of selected orientations for nanoparticles with different shapes and the resulting crystallographic directions.

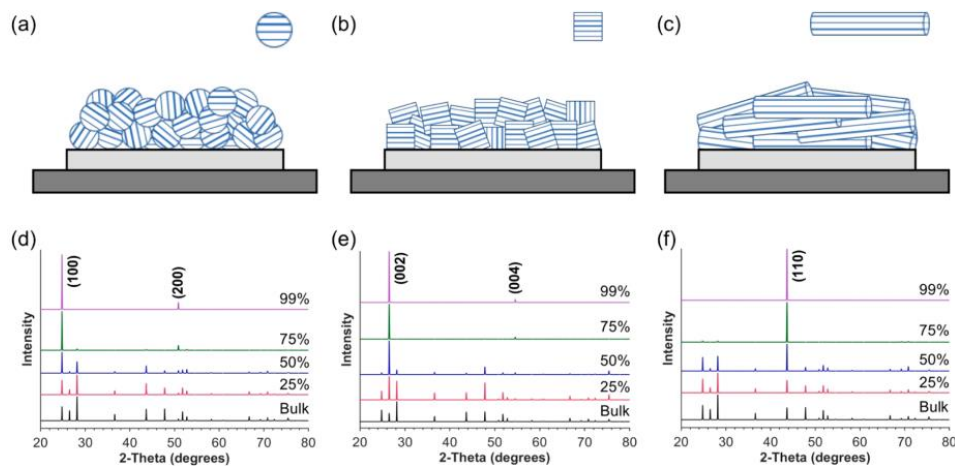


Fig. 2. Graphical representation of the preferred orientation for nanoparticles having different shapes (a) sphere, (b) cube, and (c) rod, and the resulting crystallographic directions: (d) [100], (e) [001], and (f) [110]

Furthermore, regarding the function of XRD in mixture identification and chemical analysis, XRD produces X-ray diffraction from samples indicating a crystal structure of magnesium compound materials, such as magnesium oxide (MgO), magnesium hydroxide (Mg(OH)₂), or other magnesium compounds. A study has been conducted involving XRD analysis of magnesium powder (Mg) samples in biphasic calcium phosphate (BCP) (Mg-BCP), both newly synthesized and after calcination at high temperatures of 600°C, containing crystal phases of hydroxyapatite (HA) and beta-tricalcium phosphate (β-TCP) (Moslim et al., 2018). Figure 3. shows the crystal phases of hydroxyapatite (HA) and beta-tricalcium phosphate (β-TCP) newly synthesized and after calcination at high temperatures of 600°C.

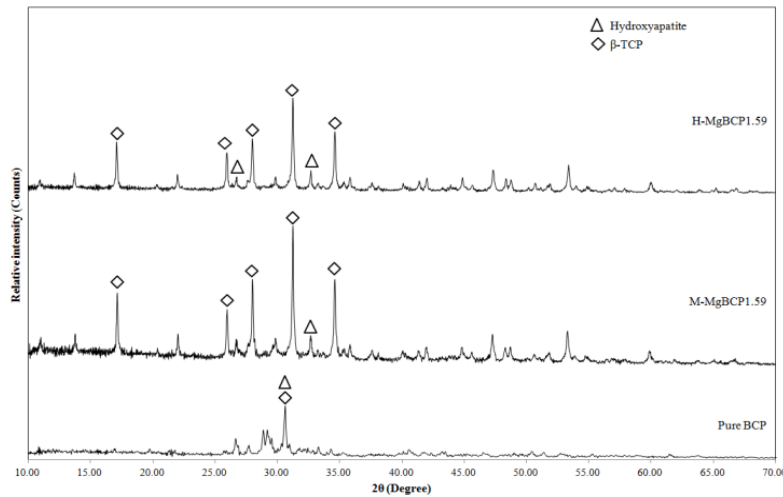


Fig. 3. Crystal phases of hydroxyapatite (HA) and beta-tricalcium phosphate (β -TCP) newly synthesized and after calcination at high temperature of 600°C.

The working principle is that X-rays emitted from a metal have a specific wavelength, and by varying the angle of reflection, elastic reflection occurs, which can be detected. X-rays are generated by the interaction between external electron beams and electrons in the atomic shell. The X-ray spectrum has wavelengths ranging from 10^{-10} to 10^{-8} meters, frequencies of 1017-1020 Hz, and energies of 103-106 electron volts. The wavelength of X-rays is of the same order as the distance between atoms, making them suitable as a source of crystal diffraction (Doumeng et al., 2021). With such capabilities, X-rays are utilized to analyze sub-kite features of hexagonal solid anions and cations to produce CoS and MnS wurtzite-type (Fatimah et al., 2021).

Furthermore, XRD technique can be used to measure crystallinity degree (Tsoukalou et al., 2019) and crystal size (Fatimah et al., 2021). In determining crystal size, XRD technique can also employ a calculation method known as the Scherrer method (Boukir et al., 2019). Additionally, XRD equipment can be utilized to determine the structural evolution of nanoparticles (Biswas et al., 2018). Moreover, the use of XRD equipment extends to determining the coexistence of two material properties (Zhang et al., 2019; Deepak et al., 2021).

Material analysis techniques using XRD can be applied to various types of materials, including metals, intermetallics, ceramics, minerals, polymers, plastics, or other inorganic or organic compounds. This analysis technique is particularly recommended for metallic materials because they have well-defined atomic structures, making them easier to analyze. In several studies, XRD analysis techniques have been employed on magnesium materials during tensile-compression deformation (Sangeetha et al., 2017) and biodegradable rare earth magnesium alloys (Sun et al., 2022). However, this analysis technique can also be applied to polymer materials, such as Poly(Vinylidene-co-Hexafluoropropylene) (PVDF-HFP) (Ahmed et al., 2022), poly(methyl methacrylate) (PMMA) (*10 - Materials Characterization.Pdf*, 1998), polyvinyl alcohol (PVA) (Powell et al., 2016), and so on.

Magnesium alloy materials are susceptible to high temperatures, as they can alter the characteristic properties of the material. Researchers continue to analyze phenomena that may occur in magnesium alloy materials at high temperatures, such as the addition of Ca and Y elements (Fan et al., 2012), the influence of material densification at high pressure (Chen, 2012), high-temperature flow behavior considering strain effects (Changizian et al., 2012; D.-H. Yu, 2013), the effect of Y element presence on the high-temperature oxidation resistance of magnesium alloys (X. Yu et al., 2016), and so forth. Recent studies have investigated high-temperature thermal phenomena of alloy structural elements, the presence of LPSO phases, favorable reinforcement phase particle morphologies, and the presence of zirconium (an active anti-solidification substance) in maintaining the high mechanical properties of the alloy (Volkova et al., 2021). Figure 4. shows backscattered electron images of three mold samples.

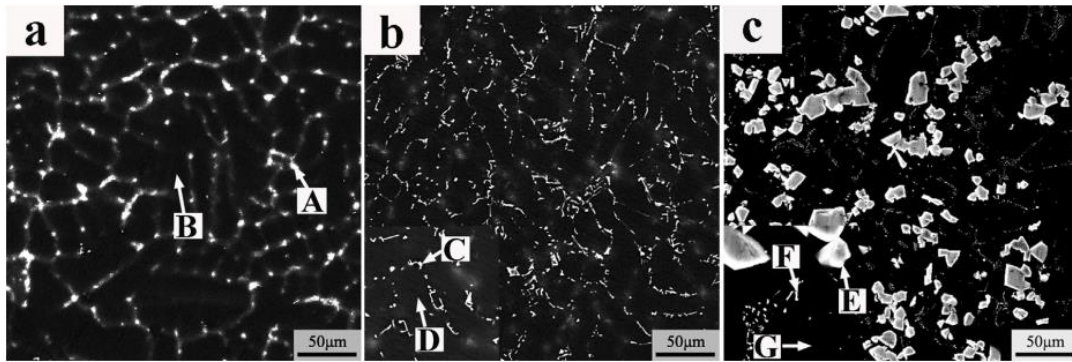


Fig. 4. Backscattered electrons of three molded samples: (a) Mg-2.5Y, (b) Mg-2.5Y-2.5Al, (c) Mg-2.5Y-4.2Al.

Many types of magnesium alloys have been studied, depending on their applications. Another application of magnesium alloy material is as batteries. In its application as batteries, one commonly used type is the magnesium alloy material AZ31 or AZ31B (Zhao et al., 2009). These types of materials are chosen because they are easy to synthesize and affordable. Recently, researchers have been striving to improve the performance of these materials. Some of the efforts include constant current density treatments of up to 40 mA cm^{-2} (Nakatsugawa & Chino, 2020), the effect of Ce content on air casting of magnesium battery anodes (Li et al., 2022), refining grain size, reducing dislocation density, and lowering grain orientation (Wang et al., 2021), and providing thin Mg foil anodes enabling the development of batteries with high energy density (Maddegalla et al., 2021). Figure 5. depicts the process of producing AZ31 magnesium alloy material that has been treated to refine grain size, reduce dislocation density, and lower grain orientation.

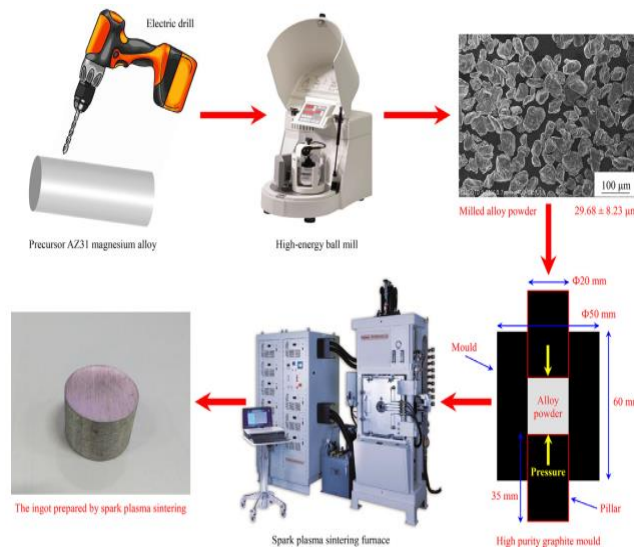


Fig. 5. The manufacturing process of AZ31 magnesium alloy material has been treated with grain refinement, low dislocation density, and low grain orientation.

Magnesium material is known for its low density, high strength, high elastic modulus, good heat dissipation, and so forth. In its applications, this material is widely used in various engineering fields, especially in seawater battery electrode anodes. However, there are some weaknesses in this material, namely its inability to withstand high temperatures. This limitation is partly due to the material's melting point. Therefore, additional composite materials are needed to enhance the material's performance at high temperatures. In this study, one of the synthesized magnesium alloy materials was subjected to a high-temperature environment to analyze the chemical compounds formed on the material. XRD equipment was used in this study to analyze the chemical compounds formed after exposure to high temperatures.

2. Research Methods

2.1 Material

In this study, an attempt was made to synthesize AZ31B magnesium alloy material using materials available in the market, including magnesium powder, aluminum, tin, and manganese. The materials used in this study were magnesium powder and additional chemical compounds used to prepare magnesium composite materials. Figure 6. illustrates the constituent materials used in this study. Some of the constituent elements of AZ31B magnesium alloy material, based on references, consist of several elements such as Mg-6Al-1Sn-0.4 (Zheng et al., 2018). According to the research results, synthesizing magnesium alloy material with this composition yielded good results at low cost, non-toxic, and performed well. Additional chemical compounds added to the magnesium powder were carefully selected according to the purpose of this experiment. However, in this study, there were some compositions modified based on previous research findings. Table 1 shows the experimental design conducted in this study.



Fig. 6. The constituent materials used in this study; a) Magnesium powder, b) Aluminum powder, c) Tin powder, and d) Manganese powder.

Table 1 - The experimental design used in this study

Sample Type	Composition of Sample Material (wt.-%)			
	Mg	Al	Sn	Mn
Sample 1	80	4	1,2	14,8
Sample 2	80	4	1	15
Sample 3	80	4	0,8	15,2
Sample 4	80	4	0,6	15,4
Sample 5	80	4	0,4	15,6

2.2 Specimen preparation

In this study, the technique used in the preparation of research specimens is powder metallurgy. Powder metallurgy is relatively easy and straightforward in its application. This technique does not require complex equipment or high costs, making it easily accessible and applicable. Powder metallurgy is known for its ability to achieve homogeneous powder mixing. The mixing and compaction processes ensure that the base metal powders and additional compounds are evenly mixed, resulting in consistent distribution of elements in the composite material. This is crucial to obtain consistent and reliable results in research on the effects of heating on the chemical structure of magnesium composite materials. By using powder metallurgy techniques, researchers can easily control the chemical composition of the resulting composite materials.

The first step in specimen preparation is the weighing of materials according to the composition in Table 1. Once these materials are weighed, they are then placed into a planetary ball mill. The use of a planetary ball mill for powder mixing holds significant importance, particularly in the context of research on magnesium composite materials. The planetary motion of the rotating and vibrating jar, along with grinding balls inside it, creates strong collision and friction forces among the powder particles. This process ensures better and more homogeneous mixing, allowing for a uniform distribution of alloying elements within the magnesium matrix. Additionally, besides achieving homogenous mixing, the planetary ball mill can also reduce the size of powder particles. Uniform particle size is crucial to ensure good physical contact between the base metal particles and alloying elements, facilitating better and more homogeneous reactions during high-temperature heating processes.

Once the powder is thoroughly mixed, pelletization is performed to form specimens into pellets of specific sizes. The pellet diameter is a key parameter to consider in the pelletization process. The pellet diameter affects the surface area and volume of material involved in reactions during heating, as well as influencing heat transfer rates and chemical reactions within the specimens. Various literature suggests different pellet diameter sizes for magnesium materials, including 6.35 mm for molding methods, 6.00 mm or 25.4 mm for briquetting methods depending on die size, and 12 mm for extrusion methods (Chubukov et al., 2018). Similarly, various studies on magnesium material for seawater batteries have used different pellet sizes ranging from 11.28 mm (Ma et al., 2020), 15 mm (Tong et al., 2021), 16 mm (Zheng et al., 2018), and so forth. However, generally, a diameter of 11.28 mm is required (Ma et al., 2020). Therefore, in this study, a pellet diameter of 11.28 mm was used. The compression strength applied to the specimen refers to previous references (Ruzuqi et al., 2021). After the pelletization process, the specimens are formed perfectly. Physical measurements are then conducted on the specimens.

Following the measurements, the specimens are placed into a furnace at a temperature of 750°C and held for 1 hour to determine the material properties under high-temperature treatment. The selection of the temperature is also based on several literature references, ranging from 720°C (Tong et al., 2021), 740°C (Zheng et al., 2018), 750°C (Ma et al., 2020), and so on. However, in this study, the temperature selection is based on the highest value previously tested to determine the maximum temperature the material can withstand. Figure 7. illustrates the process of preparing magnesium alloy material.



A



B



C



D



E



F

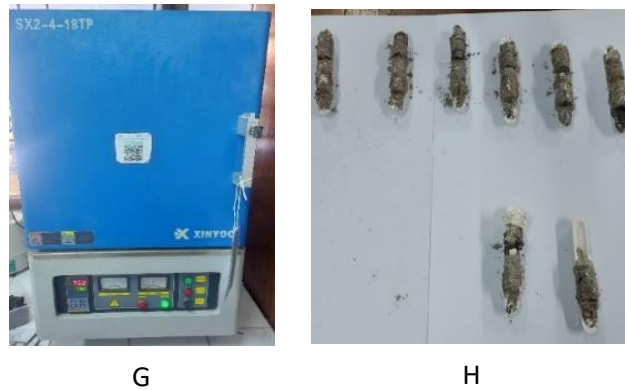


Fig. 7. Magnesium alloy material preparation process; a) Weighing of materials, b) Mixing of materials using a planetary ball mill, c) Pelletization, d) Weighing of test specimens, e) Measurement of specimen length, f) Measurement of specimen diameter, g) Heating of specimens, and h) Results.

2.3 Test Method

In this study, the testing method conducted on the specimens is XRD testing. This testing method, in addition to being used to study crystallographic structure including crystal systems, crystal quality, crystal symmetry, determining crystal defects, and finding crystal parameters, is also used for mixture identification and chemical analysis formed in the material. Therefore, in this study, this mechanism is utilized to analyze the chemical composition formed due to subjecting the material to a high temperature treatment of 750°C. XRD equipment is a technique that can be used to analyze various forms of solid materials. Therefore, in this research, the tested solid sample form is in powder form. Then, the testing angle applied is a long angle of 90°.

The results of the XRD testing are presented in the form of a diffraction pattern graph of the material which has several peak points at specific angles. The results can also be displayed in the form of a table containing information about "Pos. [°2Th.]" in the context of XRD indicating the relative position of the diffraction peak in the diffraction pattern, measured as the 2Theta angle. Then, "Height [cts]" or "Height [cts]" is the number of counts recorded by the detector at a specific position in the XRD diffraction pattern. This provides information about how strong or weak the diffraction of the crystal phase is at the given 2Theta angle. Furthermore, "FWHM Left [°2Th.]" provides information about the width of the diffraction peak on the left side of the diffraction peak in the XRD diffraction pattern at the given 2Theta angle. Then, "d-spacing [Å]" provides information about the distance between crystal lattice planes contributing to diffraction at a certain 2θ angle. This gives clues about the atomic arrangement in the crystal and the overall crystal structure. Finally, "Rel. Int. [%]" or "Relative Intensity [%]" in the context of X-ray diffraction (XRD) refers to the relative intensity of diffraction peaks in the diffraction pattern, measured in percentage. This indicates the relative contribution of the crystal phase at a specific position in the diffraction pattern.

Furthermore, the XRD test results in the form of a diffraction pattern graph are analyzed for the chemical compounds formed using MATCH software. MATCH is one of the software used in X-ray diffraction (XRD) pattern analysis to identify crystal phases in solid samples. This software contains diffraction patterns from various common sources for X-ray diffraction (XRD) pattern analysis, and the data sources can come from internal databases, public databases, and experimental data. Based on these data sources, the software can be used to identify phases. Therefore, the diffraction pattern graph obtained in the XRD testing is easy to analyze. Figure 8. shows the XRD equipment used in this study.



Fig. 8. XRD Equipment Used.

3. Results and Discussions

3.1 Results

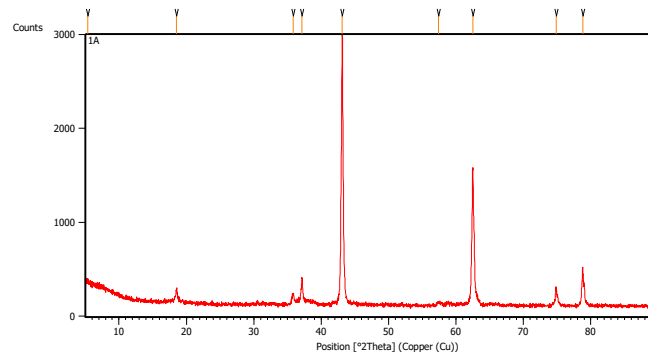
After conducting the testing using XRD equipment, peaks were obtained at several angles (2θ) passed through. The research results indicate that in five samples analyzed, four of them showed similar diffraction patterns after heating at high temperatures, but with varying intensities. Meanwhile, one sample showed a significantly different diffraction pattern from all other samples. However, for this particular sample, the compounds formed after the high-temperature heating process were almost the same as during the synthesis process. In contrast to the other four samples, the compounds formed due to the high-temperature heating process changed. This indicates the possibility of substantial changes in the chemical compounds in the magnesium composite material that need further investigation.

Then, sample 1 showed several peaks at various angles (2θ), indicating that the tested sample contained a crystal structure that reflected the emitted X-rays. These angles include 5.3425° , 18.5469° , 35.8158° , 37.1461° , 43.1238° , 57.4188° , 62.5206° , 74.8484° , and 78.7884° . Table 2 shows several peaks formed in sample 1.

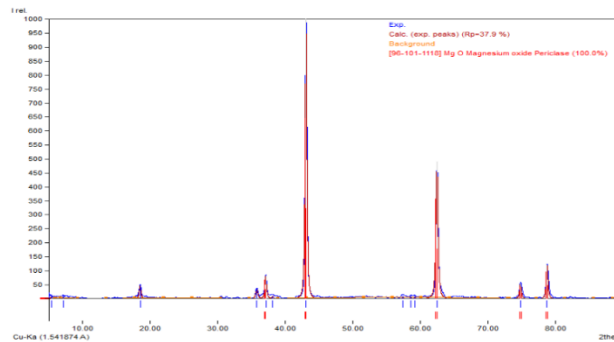
Table 2 - XRD test results table

Pos. [2θ .]	Height [cts]	FWHM Left [2θ .]	d-spacing [\AA]	Rel. Int. [%]
5.3425	42.91	0.8029	16.54172	1.49
18.5469	143.77	0.2007	4.78408	5.00
35.8158	97.36	0.3346	2.50721	3.39
37.1461	269.06	0.1338	2.42042	9.36
43.1238	2874.56	0.1506	2.09775	100.00
57.4188	29.41	0.5353	1.60489	1.02
62.5206	1449.91	0.1338	1.48564	50.44
74.8484	186.72	0.1338	1.26859	6.50
78.7884	408.54	0.1224	1.21373	14.21

Next, these angles are plotted into a graph, which is then analyzed using software. Figures 9a and 9b respectively show the graphical plot from Table 2 and the analysis results using the software. From the displayed graph, the analysis using the software reveals that these peaks form the chemical compound MgO (Magnesium Oxide Periclase) with a peak similarity value of 37.9%. These results indicate that sample 1 undergoes significant chemical reactions when subjected to high temperatures, resulting in the formation of other chemical compounds due to the high-temperature treatment.



a



b

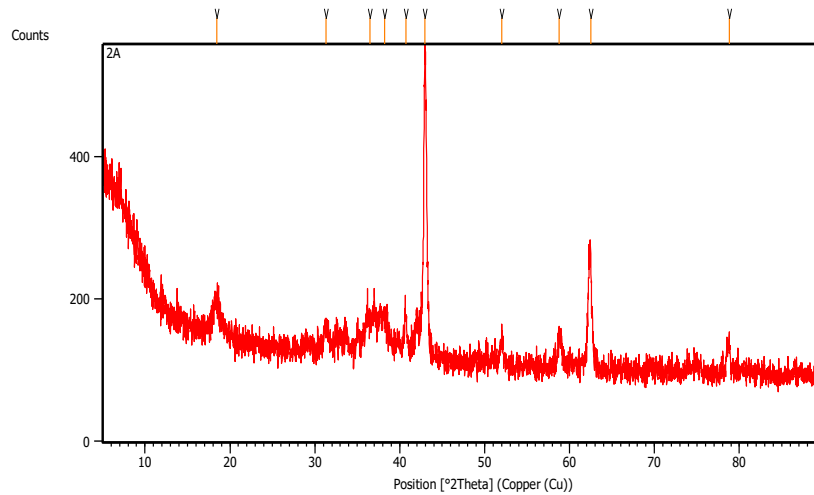
Fig. 9. XRD test results on sample 1; a) Graphical plot of Table 1 XRD test results, b) Analysis results using software.

Furthermore, for sample 2, based on the XRD testing results, peaks were obtained at several angles (2θ) passed through. These peaks indicate the presence of a crystal structure in the tested sample that reflects the emitted X-rays. Some of these angles include 18.4431° , 31.2893° , 36.5186° , 38.1781° , 40.6953° , 42.9813° , 51.9782° , 58.7359° , 62.4992° , and 78.7972° . Table 3 shows several peaks formed in sample 2.

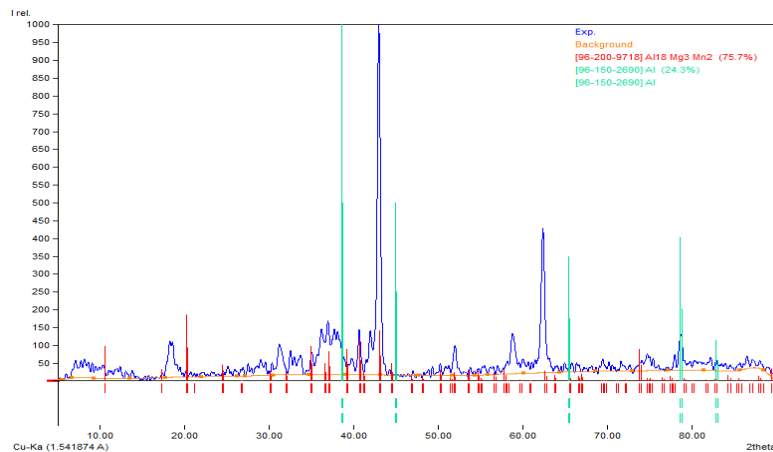
Table 3 - XRD test results table

Pos. [$^\circ 2\text{Th.}$]	Height [cts]	FWHM Left [$^\circ 2\text{Th.}$]	d-spacing [\AA]	Rel. Int. [%]
18.4431	43.30	0.6691	4.81078	10.31
31.2893	32.02	0.6691	2.85881	7.63
36.5186	26.40	0.8029	2.46056	6.29
38.1781	35.94	1.0706	2.35734	8.56
40.6953	49.58	0.2007	2.21715	11.81
42.9813	419.86	0.3011	2.10438	100.00
51.9782	34.00	0.4015	1.75933	8.10
58.7359	38.23	0.4684	1.57201	9.11
62.4992	155.60	0.3011	1.48609	37.06
78.7972	40.43	0.4015	1.21463	9.63

Next, these angles are plotted into a graph, which is then analyzed. Figures 10a and 10b respectively show the graphical plot from Table 3 and the analysis results using the software. From the displayed graph, the analysis using the software reveals that these peaks form a new compound, namely $\text{Al}_{18}\text{Mg}_3\text{Mn}_2$, with a peak similarity value of 75.7%, and the remaining 24.3% consists of Al. These results indicate that sample 2 undergoes a relatively insignificant chemical reaction when subjected to high temperatures, resulting in the formation of other chemical compounds due to the high-temperature treatment. The compounds formed due to the high-temperature treatment are almost similar to those during the material synthesis process.



a



b

Fig. 10. XRD test results on sample 2; a) Graphical plot of Table 1 XRD test results, b) Analysis results using software.

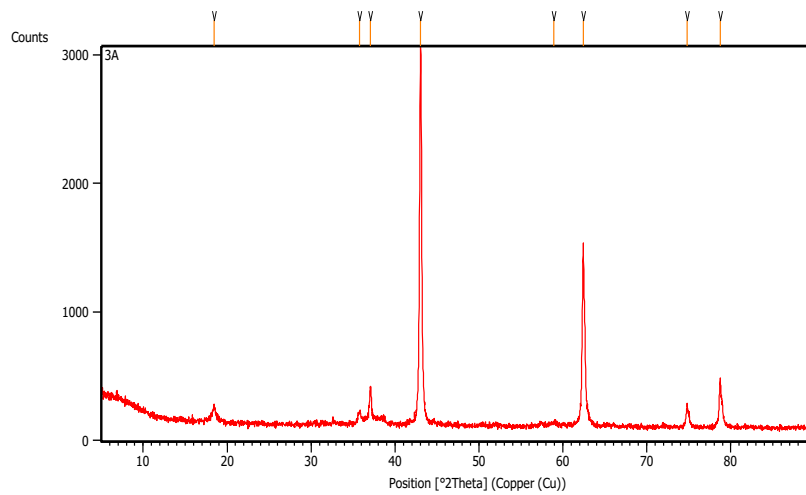
Next, for sample 3, based on the XRD testing results, peaks were obtained at several angles (2θ) passed through. These peaks indicate the presence of a crystal structure in the tested sample that reflects the emitted X-rays. Some of these angles include 18.4473° , 35.7426° , 37.0632° , 43.0357° , 58.9357° , 62.4413° , 74.7819° , and 78.7175° . Table 4 shows several peaks formed in sample 3.

Table 4 - XRD test results table

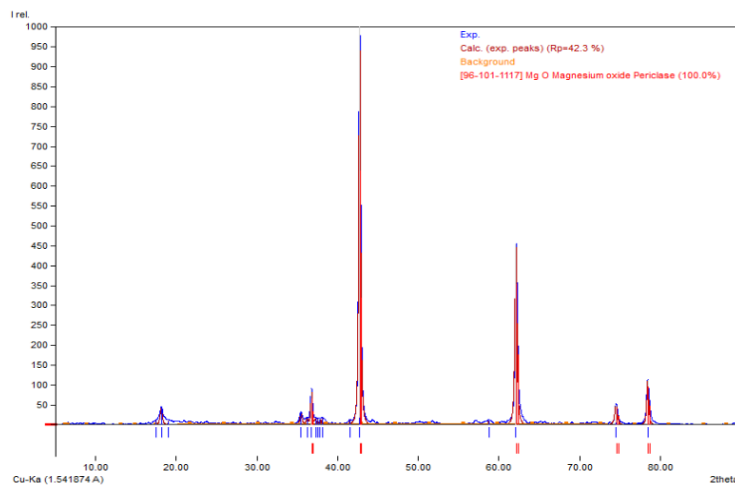
Pos. [$^\circ 2\theta$.]	Height [cts]	FWHM Left [$^\circ 2\theta$.]	d-spacing [\AA]	Rel. Int. [%]
18.4473	117.85	0.2676	4.80967	4.03
35.7426	73.64	0.3346	2.51218	2.52
37.0632	262.45	0.2007	2.42564	8.97
43.0357	2926.06	0.2175	2.10184	100.00
58.9357	19.54	0.8029	1.56715	0.67
62.4413	1403.07	0.1506	1.48733	47.95
74.7819	157.74	0.1673	1.26955	5.39
78.7175	361.94	0.1338	1.21566	12.37

Subsequently, these angles are plotted into a graph, which is then analyzed. Figures 11a and 11b respectively show the graphical plot from Table 4 and the analysis results using the software. From the displayed graph, the analysis using the software reveals that these peaks do not form a new compound, namely MgO (Magnesium Oxide Periclase). Similar to sample 1, however, in sample 3, the peak similarity value is higher than in sample 1, namely 42.3%. This means that the sample approaches the peak shape better than sample 1, which had a peak similarity of 37.9%. These results indicate that sample 3 undergoes significant chemical

reactions when subjected to high temperatures, resulting in the formation of other chemical compounds due to the high-temperature treatment compared to sample 1.



a



b

Fig. 11. XRD test results on sample 3; a) Graphical plot of Table 1 XRD test results, b) Analysis results using software.

Next, for sample 4, based on the XRD testing results, peaks were obtained at several angles (2θ) passed through. These peaks indicate the presence of a crystal structure in the tested sample that reflects the emitted X-rays. Some of these angles include 18.4341° , 31.1502° , 33.6919° , 36.1131° , 36.9995° , 42.9494° , 51.9064° , 58.7622° , 62.3798° , 62.4893° , 74.7268° , and 78.6618° . Table 5 shows several peaks formed in sample 4.

Table 5 - XRD test results table

Pos. [2θ .]	Height [cts]	FWHM Left [2θ .]	d-spacing [\AA]	Rel. Int. [%]
18.4341	114.64	0.3346	4.81311	4.58
31.1502	40.96	0.2676	2.87126	1.64
33.6919	41.31	0.2007	2.66024	1.65
36.1131	45.36	0.6691	2.48725	1.81
36.9995	269.13	0.1171	2.42968	10.74
42.9494	2504.83	0.2342	2.10586	100.00
51.9064	57.04	0.3346	1.76159	2.28
58.7622	31.78	0.6691	1.57136	1.27
62.3798	1162.07	0.1836	1.48742	46.39
62.4893	961.08	0.1224	1.48877	38.37
74.7268	136.69	0.1224	1.26930	5.46
78.6618	259.65	0.2040	1.21537	10.37

Subsequently, these angles are plotted into a graph, which is then analyzed. Figures 12a and 12b respectively show the graphical plot from Table 5 and the analysis results using the software. From the displayed graph, the analysis using the software reveals that these peaks do not form a new compound, namely MgO (Magnesium Oxide Periclase). Similar to sample 1, however, in sample 4, the peak similarity value is higher than in samples 1 and 3, namely 43.3%. This means that the sample approaches the peak shape better than samples 1 and 3, which had peak similarities of 37.9% and 42.3%, respectively. These results indicate that sample 4 undergoes significant chemical reactions when subjected to high temperatures, resulting in the formation of other chemical compounds due to the high-temperature treatment compared to samples 1 and 3.

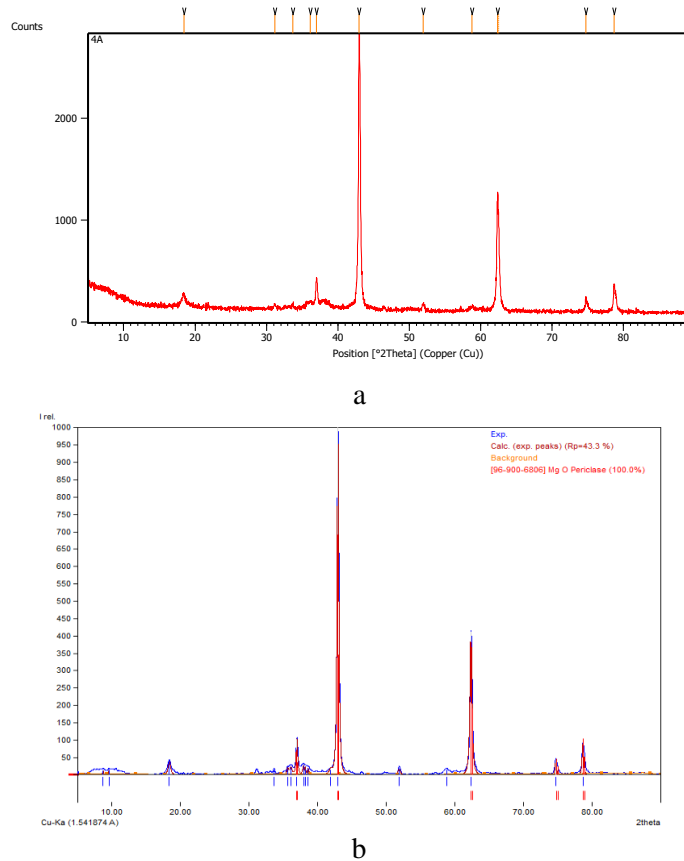


Fig. 12. XRD test results on sample 4; a) Graphical plot of Table 1 XRD test results, b) Results of analysis using software.

Finally, in this study, for sample 5, based on the XRD testing results, peaks were obtained at several angles (2θ) passed through. These peaks indicate the presence of a crystal structure in the tested sample that reflects the emitted X-rays. Some of these angles include 18.3903°, 31.1730°, 33.7750°, 36.2098°, 37.0386°, 40.6732°, 42.0406°, 43.1243°, 46.8610°, 52.0321°, 58.7688°, 62.4269°, 74.7776°, and 78.7052°. Table 6 shows several peaks formed in sample 5.

Table 6 - XRD test results table

Pos. [$^{\circ}2\theta$.]	Height [cts]	FWHM Left [$^{\circ}2\theta$.]	d-spacing [\AA]	Rel. Int. [%]
18.3903	43.56	0.5353	4.82446	4.09
31.1730	56.90	0.2676	2.86921	5.35
33.7750	64.73	0.2676	2.65389	6.08
36.2098	60.57	0.2676	2.48083	5.69
37.0386	99.58	0.2676	2.42720	9.36
40.6732	37.02	0.4015	2.21830	3.48
42.0406	94.81	0.2676	2.14926	8.91
43.1243	1064.31	0.1338	2.09773	100.00
46.8610	18.66	0.8029	1.93880	1.75
52.0321	99.04	0.2676	1.75763	9.31
58.7688	32.48	0.5353	1.57120	3.05

62.4269	509.95	0.2676	1.48764	47.91
74.7776	57.67	0.4015	1.26962	5.42
78.7052	134.05	0.2676	1.21581	12.60

Subsequently, these angles are plotted into a graph, which is then analyzed. Figures 13a and 13b respectively show the graphical plot from Table 6 and the analysis results using the software. From the displayed graph, the analysis using the software reveals that these peaks do not form a new compound, namely MgO (Magnesium Oxide Periclase). Similar to sample 1, however, in sample 5, the peak similarity value is higher than in samples 1, 3, and 4, namely 63.0%. This means that the sample approaches the peak shape better than samples 1, 3, and 4, which had peak similarities of 37.9%, 42.3%, and 43.3%, respectively. These results indicate that sample 5 undergoes significant chemical reactions when subjected to high temperatures, resulting in the formation of other chemical compounds due to the high-temperature treatment compared to samples 1, 3, and 4.

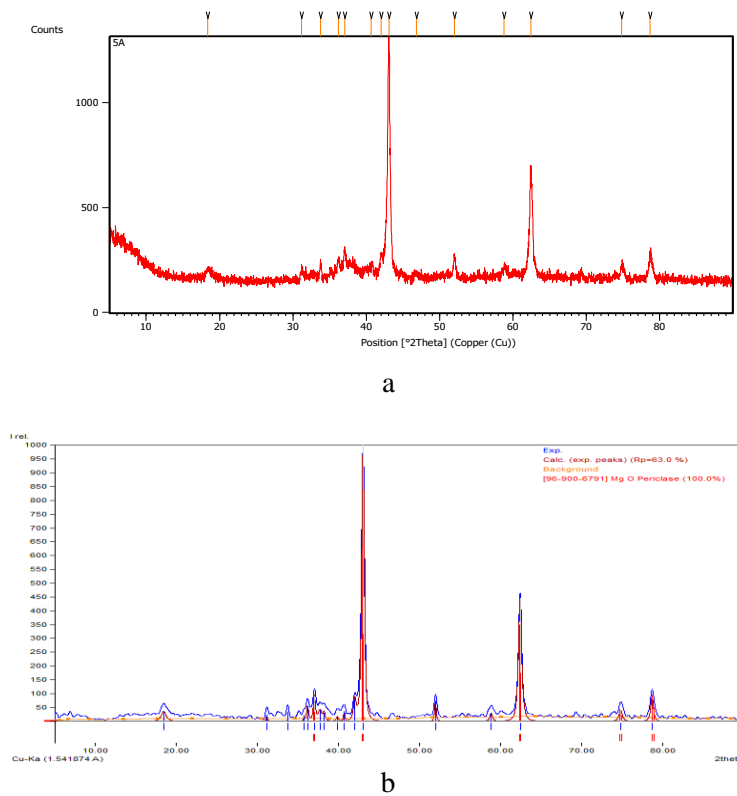


Fig. 13. XRD test results on sample 5; a) Graphical plot of Table 1 XRD test results, b) Analysis results using software.

3.2. Discussion

Changes in compounds in a material are natural occurrences, and generally, some causes of these changes include heating or thermal treatment, which can lead to changes in crystal phases, decomposition, or chemical reactions between material components. Furthermore, interaction with the environment, such as reacting with surrounding materials like air, water, or specific chemicals, can also occur. These reactions can result in the formation of oxide layers, corrosion, or other chemical changes on the material's surface. Additionally, contamination or pollution by external substances can cause changes in material properties. Contaminants like dust, foreign particles, or chemicals can alter the composition or structure of the material and affect its performance. Mechanical deformation, such as applying stress, mechanical processing, or plastic deformation, can lead to changes in crystal structure, dislocations, or cracks in the material. Moreover, interactions with other materials within a system or specific environment can trigger chemical reactions or structural changes. This can occur during processes like welding, alloying, or material blending. Furthermore, variations in temperature and pressure can also affect the structure and properties of materials. Increasing temperature or pressure can trigger chemical reactions or phase changes in materials. Lastly, over time, changes in materials

can occur due to aging processes, thermal degradation, or slow chemical reactions within the material system.

Based on the test results, it was found that four samples formed magnesium oxide (MgO) (Magnesium Oxide Periclase) compounds, and one sample formed the compound $Al_{18}Mg_3Mn_2$ along with aluminum. These results indicate significant chemical compound changes in most samples due to high-temperature treatment. The MgO (Magnesium Oxide Periclase) compound resulting from these changes is a type of magnesium mineral found naturally in metamorphic rocks. This mineral is a major component of most basic refractory rocks used in various industrial applications, particularly in the metallurgical and refractory industries. Typically, magnesium oxide is obtained by removing water from magnesium hydroxide (Mg(OH)₂) through a dehydration process and has been intensively studied using X-ray diffraction techniques (Terauchi et al., 1980; Guillatt & Brett, 1971). Meanwhile, the $Al_{18}Mg_3Mn_2$ compound is obtained from an induction melting process using pure constituent elements (Al, 99.9%; Mg, 99.9%, and Mn, 99.9%) under an inert argon atmosphere. Rapid solidification of such cast alloys is carried out using a spin casting unit in a controlled atmosphere with argon flow (Mukhopadhyay et al., 2008).

Furthermore, based on the test results, these changes can be attributed to common causes such as heating or thermal treatment, reactions with the environment, and external factors. Concerning changes due to heating or thermal treatment in the tested samples, each material has its characteristics, including melting points and chemical reactions at different temperatures. For instance, the samples consist of several materials with different melting point characteristics, such as magnesium at 650°C, aluminum at 660°C, tin at 231°C, and manganese at 1246°C. Based on these characteristics, it is evident that at the high temperature of 750°C applied in this study, several elements may melt and undergo chemical reactions with each other, resulting in chemical compound changes.

Additionally, changes in compounds due to reactions with the surrounding environment, such as air, were not prevented during the high-temperature treatment process. In this study, no specific treatments were applied to prevent the materials from reacting with the air, such as using inert gas. In this context, inert gas is necessary to help prevent oxidation, protect the surface, and control the atmosphere. Inert gas refers to a type of gas that does not chemically react with other substances under normal conditions. Inert gases tend to be stable and non-reactive chemically under various conditions. Therefore, these gases are commonly used in various applications, including industries, technology, and science. For example, in welding, inert gas, such as argon, is needed to protect the arc and metal from reacting with oxygen in the air (Baeva et al., 2019).

Lastly, external factors, such as XRD equipment, can also cause changes in compounds. The working principle of XRD (X-Ray Diffraction) equipment is based on X-ray diffraction by solid crystals. In XRD, X-rays are emitted into the sample, and the interaction of X-rays with the crystal structure in the sample produces characteristic diffraction patterns reflecting the atomic arrangement in the sample. During this process, X-rays may be emitted onto the sample with its chemical composition. This can occur because the tested sample is in powder form scattered in the XRD equipment's test container. Due to the working principle of XRD equipment, only one point becomes the center of analysis for the XRD equipment. Therefore, this possibility can occur during the compound analysis process in the sample, leading to the formation of new compounds

4. Conclusion

From several samples tested in this research, it was found that the majority of magnesium composite material samples undergo significant chemical compound changes when exposed to high-temperature environments. The initial materials composed of MgAlSnMn transformed into compounds such as MgO (Magnesium Oxide Periclase), the compound $Al_{18}Mg_3Mn_2$, and elemental Al. The changes were observed in four samples forming MgO (Magnesium Oxide Periclase) compounds, while one sample formed the compound $Al_{18}Mg_3Mn_2$ along with elemental Al. Among the four materials forming MgO (Magnesium Oxide Periclase) compounds, there were differences only in the peak similarity percentage based on the analysis

results using Match software, with samples 1, 3, 4, and 5 at 37.9%, 42.3%, 43.3%, and 63.0%, respectively. The highest similarity percentage was obtained in sample 5, which was 63.0% of the MgO (Magnesium Oxide Periclase) compound. Meanwhile, in sample 2, the similarity percentage of the material with the compound $\text{Al}_{18}\text{Mg}_3\text{Mn}_2$ based on Match software analysis was 75.7%, with the remaining having a similarity with elemental Al at 24.3%.

Based on the research results, the causes of chemical compound changes are heating or thermal treatment and reactions with the environment. The compounds formed from high-temperature heating may potentially disrupt the performance of magnesium composite anode electrodes in seawater batteries when applied. Additionally, environmental reaction factors during high-temperature exposure, such as materials without inert gas supply, also lead to significant chemical compound changes. In this study, minor changes were made in the material synthesis process. Because a battery serves as an energy source for electronic devices, especially for seawater batteries, which offer extensive research opportunities to address challenges and enhance the performance and large-scale application of seawater batteries to support the transition towards clean and sustainable energy. Therefore, further research is expected in the future on the best material compositions in magnesium composites or even other treatments provided, to improve the quality and performance of products.

Acknowledgement

In this research, the authors would like to express their gratitude to the person in charge of the Materials and Energy Laboratory of the Sorong Marine and Fisheries Research Polytechnic and the Metallurgical Engineering Study Program of the Sepuluh Nopember Institute of Technology Surabaya who have supported this work

References

- Ahmed, M. B., Nofal, M. M., Aziz, S. B., Al-Saeedi, S. I., Brza, M. A., Dannoun, E. M. A., & Murad, A. R. (2022). The study of ion transport parameters associated with dissociated cation using EIS model in solid polymer electrolytes (SPEs) based on PVA host polymer: XRD, FTIR, and dielectric properties. *Arabian Journal of Chemistry*, 15(11), 104196. <https://doi.org/10.1016/j.arabjc.2022.104196>
- Baeva, M., Loffhagen, D., & Uhrlandt, D. (2019). Unified Non-equilibrium Modelling of Tungsten-Inert Gas Microarcs in Atmospheric Pressure Argon. *Plasma Chemistry and Plasma Processing*, 39(6), 1359–1378. <https://doi.org/10.1007/s11090-019-10020-x>
- Biswas, R. K., Khan, P., Mukherjee, S., Mukhopadhyay, A. K., Ghosh, J., & Muraleedharan, K. (2018). Study of short range structure of amorphous Silica from PDF using Ag radiation in laboratory XRD system, RAMAN and NEXAFS. *Journal of Non-Crystalline Solids*, 488, 1–9. <https://doi.org/10.1016/j.jnoncrysol.2018.02.037>
- Boukir, A., Fellak, S., & Doumenq, P. (2019). Structural characterization of *Argania spinosa* Moroccan wooden artifacts during natural degradation progress using infrared spectroscopy (ATR-FTIR) and X-Ray diffraction (XRD). *Heliyon*, 5(9), e02477. <https://doi.org/10.1016/j.heliyon.2019.e02477>
- Changizian, P., Zarei-Hanzaki, A., & Roostaei, A. A. (2012). The high temperature flow behavior modeling of AZ81 magnesium alloy considering strain effects. *Materials & Design*, 39, 384–389. <https://doi.org/10.1016/j.matdes.2012.02.049>
- Chen, G. H. (2012). Effect of High-Pressure Solution Temperature on Corrosion Resistance of AM60 Magnesium Alloy. *Advanced Materials Research*, 580, 560–563. <https://doi.org/10.4028/www.scientific.net/AMR.580.560>
- Chubukov, B. A., Palumbo, A. W., Rowe, S. C., Wallace, M. A., Sun, K. Y., & Weimer, A. W. (2018). Design and Fabrication of Pellets for Magnesium Production by Carbothermal Reduction. *Metallurgical and Materials Transactions B*, 49(5), 2209–2218. <https://doi.org/10.1007/s11663-018-1309-5>
- Deepak, J. R., Arunkumar, T., Ravipati, S. V. S. D., & Varma, S. S. S. K. S. (2021). XRD investigation of biodegradable magnesium rare earth alloy. *Materials Today: Proceedings*, 47, 4676–4681. <https://doi.org/10.1016/j.matpr.2021.05.542>

- Doumeng, M., Makhlof, L., Berthet, F., Marsan, O., Delbé, K., Denape, J., & Chabert, F. (2021). A comparative study of the crystallinity of polyetheretherketone by using density, DSC, XRD, and Raman spectroscopy techniques. *Polymer Testing*, *93*, 106878. <https://doi.org/10.1016/j.polymeresting.2020.106878>
- Fan, J., Yang, C., & Xu, B. (2012). Effect of Ca and Y additions on oxidation behavior of magnesium alloys at high temperatures. *Journal of Rare Earths*, *30*(5), 497–502. [https://doi.org/10.1016/S1002-0721\(12\)60079-9](https://doi.org/10.1016/S1002-0721(12)60079-9)
- Fatimah, S., Ragadhita, R., Husaeni, D. F. A., & Nandiyanto, A. B. D. (2021). How to Calculate Crystallite Size from X-Ray Diffraction (XRD) using Scherrer Method. *ASEAN Journal of Science and Engineering*, *2*(1), 65–76. <https://doi.org/10.17509/ajse.v2i1.37647>
- Guilliatt, I. F., & Brett, N. H. (1971). Crystallite size and shape relationships in the product-precursor pair MgO-Mg(OH)₂. *Philosophical Magazine*, *23*(183), 647–653. <https://doi.org/10.1080/14786437108216410>
- Holder, C. F., & Schaak, R. E. (2019). Tutorial on Powder X-ray Diffraction for Characterizing Nanoscale Materials. *ACS Nano*, *13*(7), 7359–7365. <https://doi.org/10.1021/acsnano.9b05157>
- Li, Q., Xiong, W., Yu, M., Li, J., Liu, L., Zhu, G., Wang, L., Wang, J., Yu, S., & Liu, E. (2022). Effect of Ce content on performance of AZ31 magnesium alloy anode in air battery. *Journal of Alloys and Compounds*, *891*, 161914. <https://doi.org/10.1016/j.jallcom.2021.161914>
- Ma, J., Zhang, Y., Ma, M., Qin, C., Ren, F., & Wang, G. (2020). Corrosion and discharge performance of a magnesium aluminum eutectic alloy as anode for magnesium–air batteries. *Corrosion Science*, *170*, 108695. <https://doi.org/10.1016/j.corsci.2020.108695>
- Maddegalla, A., Mukherjee, A., Blázquez, J. A., Azaceta, E., Leonet, O., Mainar, A. R., Kovalevsky, A., Sharon, D., Martin, J., Sotta, D., Ein-Eli, Y., Aurbach, D., & Noked, M. (2021). AZ31 Magnesium Alloy Foils as Thin Anodes for Rechargeable Magnesium Batteries. *ChemSusChem*, *14*(21), 4690–4696. <https://doi.org/10.1002/cssc.202101323>
- Moslim, N. A., Ahmad, N., & Kasim, S. R. (2018). XRD Analysis of Calcined Magnesium Substituted Biphasic Calcium Phosphate (Mg-BCP). *Journal of Physics: Conference Series*, *1082*, 012025. <https://doi.org/10.1088/1742-6596/1082/1/012025>
- Mukhopadhyay, N. K., Chang, H. J., Lee, J. Y., & Kim, D. H. (2008). Electron microscopy of an icosahedral phase in a rapidly solidified Al18Mg3Mn2 complex metallic alloy. *Scripta Materialia*, *59*(10), 1119–1122. <https://doi.org/10.1016/j.scriptamat.2008.07.024>
- Nakatsugawa, I., & Chino, Y. (2020). Performance of AZ31 Alloy as Anodes for Primary Magnesium-Air Batteries under High Current Discharge. *MATERIALS TRANSACTIONS*, *61*(1), 200–205. <https://doi.org/10.2320/matertrans.MT-M2019259>
- Powell, A. E., Hodges, J. M., & Schaak, R. E. (2016). Preserving Both Anion and Cation Sublattice Features during a Nanocrystal Cation-Exchange Reaction: Synthesis of Metastable Wurtzite-Type CoS and MnS. *Journal of the American Chemical Society*, *138*(2), 471–474. <https://doi.org/10.1021/jacs.5b10624>
- Pu, Z., Outeiro, J. C., Batista, A. C., Dillon, O. W., Puleo, D. A., & Jawahir, I. S. (2012). Enhanced surface integrity of AZ31B Mg alloy by cryogenic machining towards improved functional performance of machined components. *International Journal of Machine Tools and Manufacture*, *56*, 17–27. <https://doi.org/10.1016/j.ijmachtools.2011.12.006>
- Ruzuqi, R., Rudyardjo, M.Si., Drs. D. I., & Zaidan, S.Si., M.Si., Ph.D., A. H. (2021). Synthesis and Characterization of Nickel-Based Superalloy Materials for Manufacturing Aircraft Turbine Blades. *Indonesian Applied Physics Letters*, *2*(2), 49. <https://doi.org/10.20473/iapl.v2i2.31557>
- Sangeetha, M., Mallikarjun, A., Jaipal Reddy, M., & Siva Kumar, J. (2017). SEM, XRD and electrical conductivity studies of PVDF-HFP-LiBF₄ –EC plasticized gel polymer electrolyte. *020064*. <https://doi.org/10.1063/1.4990217>
- Singh, V. P., Patel, S. K., Ranjan, A., & Kuriachen, B. (2020). Recent research progress in solid state friction-stir welding of aluminium–magnesium alloys: A critical review. *Journal of*

- Materials Research and Technology*, 9(3), 6217–6256. <https://doi.org/10.1016/j.jmrt.2020.01.008>
- Sun, C. C., You, A. H., & Teo, L. L. (2022). XRD Measurement for Particle Size Analysis of PMMA Polymer Electrolytes with SiO₂. *International Journal of Technology*, 13(6), 1336. <https://doi.org/10.14716/ijtech.v13i6.5927>
- Terauchi, H., Ohga, T., & Naono, H. (1980). Dehydration in Mg(OH)₂. *Solid State Communications*, 35(11), 895–897. [https://doi.org/10.1016/0038-1098\(80\)91048-0](https://doi.org/10.1016/0038-1098(80)91048-0)
- Tong, F., Chen, X., Wei, S., Malmström, J., Vella, J., & Gao, W. (2021). Microstructure and battery performance of Mg-Zn-Sn alloys as anodes for magnesium-air battery. *Journal of Magnesium and Alloys*, 9(6), 1967–1976. <https://doi.org/10.1016/j.jma.2021.08.022>
- Tsoukalou, A., Abdala, P. M., Stoian, D., Huang, X., Willinger, M.-G., Fedorov, A., & Müller, C. R. (2019). Structural Evolution and Dynamics of an In₂O₃ Catalyst for CO₂ Hydrogenation to Methanol: An Operando XAS-XRD and In Situ TEM Study. *Journal of the American Chemical Society*, 141(34), 13497–13505. <https://doi.org/10.1021/jacs.9b04873>
- Volkova, E. F., Mostyaev, I. V., Akinina, M. V., & Alikhanyan, A. A. (2021). Effect of High-Temperature Heating on the Structure, Phase Composition, and Properties of Small Stampings Made of a VMD16 Magnesium Alloy. *Russian Metallurgy (Metally)*, 2021(11), 1402–1408. <https://doi.org/10.1134/S0036029521110112>
- Wang, N., Huang, Y., Liu, J., Yang, X., Xie, W., Cai, Q., Zheng, S., & Shi, Z. (2021). AZ31 magnesium alloy with ultrafine grains as the anode for Mg-air battery. *Electrochimica Acta*, 378, 138135. <https://doi.org/10.1016/j.electacta.2021.138135>
- Wu, G., Chan, K.-C., Zhu, L., Sun, L., & Lu, J. (2017). Dual-phase nanostructuring as a route to high-strength magnesium alloys. *Nature*, 545(7652), 80–83. <https://doi.org/10.1038/nature21691>
- Xu, T., Yang, Y., Peng, X., Song, J., & Pan, F. (2019). Overview of advancement and development trend on magnesium alloy. *Journal of Magnesium and Alloys*, 7(3), 536–544. <https://doi.org/10.1016/j.jma.2019.08.001>
- Yan, Z., Wang, D., He, X., Wang, W., Zhang, H., Dong, P., Li, C., Li, Y., Zhou, J., Liu, Z., & Sun, L. (2018). Deformation behaviors and cyclic strength assessment of AZ31B magnesium alloy based on steady ratcheting effect. *Materials Science and Engineering: A*, 723, 212–220. <https://doi.org/10.1016/j.msea.2018.03.023>
- Yu, D.-H. (2013). Modeling high-temperature tensile deformation behavior of AZ31B magnesium alloy considering strain effects. *Materials & Design*, 51, 323–330. <https://doi.org/10.1016/j.matdes.2013.04.022>
- Yu, W., Sun, R., Guo, Z., Wang, Z., He, Y., Lu, G., Chen, P., & Chen, K. (2019). Novel fluoridated hydroxyapatite/MAO composite coating on AZ31B magnesium alloy for biomedical application. *Applied Surface Science*, 464, 708–715. <https://doi.org/10.1016/j.apsusc.2018.09.148>
- Yu, X., Shen, S., Jiang, B., Jiang, Z., Yang, H., & Pan, F. (2016). The effect of the existing state of Y on high temperature oxidation properties of magnesium alloys. *Applied Surface Science*, 370, 357–363. <https://doi.org/10.1016/j.apsusc.2016.02.156>
- Zhang, H., Jérusalem, A., Salvati, E., Papadaki, C., Fong, K. S., Song, X., & Korsunsky, A. M. (2019). Datasets for multi-scale diffraction analysis (synchrotron XRD and EBSD) of twinning-detwinning during tensile-compressive deformation of AZ31B magnesium alloy samples. *Data in Brief*, 26, 104423. <https://doi.org/10.1016/j.dib.2019.104423>
- Zhao, H., Bian, P., & Ju, D. (2009). Electrochemical performance of magnesium alloy and its application on the sea water battery. *Journal of Environmental Sciences*, 21, S88–S91. [https://doi.org/10.1016/S1001-0742\(09\)60045-0](https://doi.org/10.1016/S1001-0742(09)60045-0)
- Zheng, T., Hu, Y., Zhang, Y., Yang, S., & Pan, F. (2018). Composition optimization and electrochemical properties of Mg-Al-Sn-Mn alloy anode for Mg-air batteries. *Materials & Design*, 137, 245–255. <https://doi.org/10.1016/j.matdes.2017.10.031>